

AAS 03-065



## Design and Analysis of the ST7 Disturbance Reduction System (DRS) Spacecraft Controller

P. G. Maghami, F. L. Markley, M. B. Houghton, C. J. Dennehy

NASA/Goddard Space Flight Center

---

26th ANNUAL AAS GUIDANCE AND CONTROL CONFERENCE

---

February 5-9, 2003  
Breckenridge, Colorado

Sponsored by  
Rocky Mountain Section



AAS Publications Office, P.O. Box 28130 - San Diego, California 92198

# **“Design and Analysis of the ST7 Disturbance Reduction System (DRS) Spacecraft Controller”**

**M. Houghton, F. L. Markley, C. J. Dennehy, P. Maghami, S. Prakash and F. Bauer**

**NASA Goddard Space Flight Center (GSFC)  
Guidance, Navigation and Control Center (GNCC)  
Greenbelt, MD 20771**

NASA's New Millennium Program (NMP) recently selected the Disturbance Reduction System (DRS) technology for the Space Technology 7 (ST7) flight validation experiment scheduled to fly in 2006. NMP missions such as ST7 are intended to validate advanced technologies that have not flown in space in order to reduce the risk of their infusion in future NASA Space Science missions. In particular, the Jet Propulsion Laboratory (JPL) managed ST7 DRS project will perform an on-orbit system-level validation of the sensor and actuator technologies required to control a vehicle's flight path through space so that the science payload responds only to gravitational forces.

Two specific DRS technologies are to be flight validated on the ST7 mission. The first technology is a highly sensitive Gravitational Reference Sensor (GRS), provided by Stanford University, that will be used to measure the position and attitude of a spacecraft with respect to an internal free-floating test mass. The second technology is a set of miniature micro-Newton colloidal thrusters, provided by the Busek Company.

The revolutionary ST7 DRS control system will provide an unprecedented level of spacecraft stabilization performance. Mission objectives require the DRS control system to maintain the spacecraft's position, with respect to the GRS free-floating test mass, to less than  $10 \text{ nm}/\sqrt{\text{Hz}}$ , over the frequency range  $10^{-3} \text{ Hz}$  to  $10^{-2} \text{ Hz}$ .

This paper presents the overall design and analysis process of the spacecraft controller that will serve to close the loop between the GRS and the micro-Newton colloidal thrusters. The spacecraft controller is currently being designed by NASA's Goddard Space Flight Center to satisfy the stringent translation control requirements for maintaining the spacecraft centered on the GRS test mass. The Linear Quadratic Gaussian (LQG) controller, which includes a Kalman Filter (KF) estimator, processes the GRS test mass position and attitude reference signals to determine the required thrust levels of the colloidal thrusters to produce the desired forces and torques on the spacecraft.

DRS control system requirements and performance goals are presented in this paper along with the overall DRS control system architecture. The 18-DOF DRS end-to-end dynamic model, developed by GSFC, is described and preliminary performance results are presented. Key controller design trades are summarized. Plans for closed loop testing of the DRS controller on GSFC's Formation Flying Test Bed (FFTB) are presented. A discussion of how the DRS technology is envisioned to be enabling or enhancing for many future NASA missions is also in this paper.

## DESIGN AND ANALYSIS OF THE ST7 DISTURBANCE REDUCTION SYSTEM (DRS) SPACECRAFT CONTROLLER

P. G. Maghami,\* F. L. Markley,\* M. B. Houghton,\* and C. J. Dennehy\*

The Space Technology 7 experiment will perform an on-orbit system-level validation of two specific Disturbance Reduction System technologies: a gravitational reference sensor employing a free-floating test mass and a set of micronewton colloidal thrusters. The Disturbance Reduction System is designed to maintain a spacecraft's position with respect to the free-floating test mass to less than  $10 \text{ nm}/\sqrt{\text{Hz}}$ , over the frequency range  $10^{-3} \text{ Hz}$  to  $10^{-2} \text{ Hz}$ . This paper presents the design and analysis of the coupled drag-free and attitude control system that closes the loop between the gravitational reference sensor and the micronewton thrusters while incorporating star tracker data at low frequencies. The effects of actuation and measurement noise and disturbances on the spacecraft and test masses are evaluated in a seven-degree-of-freedom planar model incorporating two translational and one rotational degrees of freedom for the spacecraft and two translational degrees of freedom for each test mass.

### INTRODUCTION

NASA's New Millennium Program (NMP) recently selected the Disturbance Reduction System (DRS) flight validation experiment, managed by the Jet Propulsion Laboratory (JPL), for the Space Technology 7 (ST7) mission.<sup>1</sup> NMP missions are intended to validate advanced technologies that have not flown in space in order to reduce the risk of their infusion in future NASA Space Science missions. The ST7 DRS incorporates two specific technologies: a highly sensitive Gravitational Reference Sensor (GRS), provided by Stanford University, to measure the position and attitude of a spacecraft with respect to an internal free-floating test mass, and a set of micronewton colloidal thrusters, provided by the Busek Company. The ST7 DRS, scheduled to fly on the European Space Agency's SMART-II spacecraft in 2006, is designed to maintain the spacecraft's position, with respect to the GRS free-floating test mass, to less than  $10 \text{ nm}/\sqrt{\text{Hz}}$ , over ST7's science measurement frequency range from 1 to 10 mHz. The DRS instrument package consists of two gravitational reference sensors, two sets of four microNewton thrusters each for position and attitude control, and an interferometer to measure the distance between the two test masses, as shown in Figure 1.

This paper presents the overall design and analysis process of the spacecraft controller being developed at NASA's Goddard Space Flight Center to close the loop between the GRS and the micronewton colloidal thrusters. A two-dimensional (planar) model has been developed to capture the essential dynamics of the ST7-DRS package. It includes seven rigid-body dynamic degrees of freedom: two translations and a rotation for the spacecraft, and two translations for each test mass, ignoring the inessential rotational dynamics of the test masses. Actuation and measurement noise and disturbance sources acting on the spacecraft and test masses are modeled. The ST7 DRS comprises three control systems: the attitude control system (ACS) to maintain a sun-pointing attitude; the drag free control (DFC) to center the spacecraft about the test masses; and the test mass suspension control. This paper summarizes the control design and analysis of the ST7-DRS 7-DOF model.

---

\*Guidance, Navigation and Control Division, NASA Goddard Space Flight Center, Greenbelt, MD 20771

Two disturbances are included in this model. The first is the nominal solar radiation pressure and its variation. The Sun exposed face of the spacecraft corresponds to the  $-Y$  direction. The angle of the incident rays of the sun to the surface normal,  $\alpha$ , may be arbitrarily assigned. However, it is assumed to be zero for the current analysis. The frequency spectrum used for solar radiation flux variations given in Figure 3 represents a conservative assessment of measured variations.<sup>2,3</sup> This plot indicates a constant spectrum at the frequencies below 0.1 mHz, followed by a  $1/f$  roll off. This spectrum also includes the so-called 5-minute acoustic oscillation (at 3.5 mHz), and levels off at frequencies above 10 mHz. The second disturbance source modeled was the acceleration noise on the test mass. A number of sources contribute to this acceleration noise, including magnetic and Lorentz forces, thermal disturbances, cosmic ray impacts, etc.<sup>2</sup> The spectral density function for the test mass acceleration noise is assumed to have the following characteristics:

- $1/f^2$  rolloff at frequency range of 0.01-0.1 mHz,
- $1/f$  rolloff at frequency range of 0.1-1 mHz,
- constant spectral density  $3 \times 10^{-14} \text{ m/s}^2/\text{Hz}^{0.5}$  at frequencies above 1 mHz.

In order to incorporate this power spectrum within the frequency and time domain analyses, the linear filter approximation shown in Figure 4 was developed. Note that all requirements are either met or exceeded by this approximation. This acceleration noise was applied to both test masses in all directions.

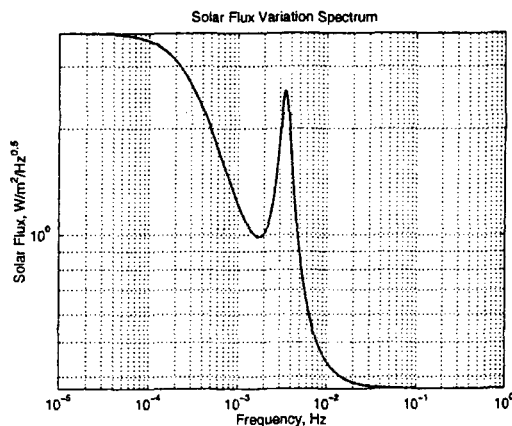


**Figure 3 Root Power Spectrum of the Solar Radiation Flux Variations**

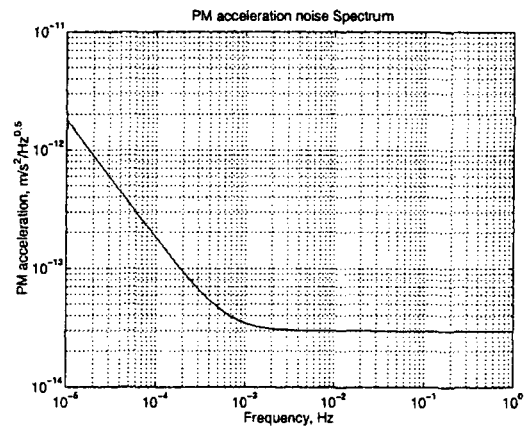


**Figure 4 Root Power Spectrum for the Test Mass Acceleration Noise**

White-noise models were used to capture thruster noise, electrostatic suspension force noise, star tracker noise, and the capacitive sensing noise (used to measure the positions of the test masses relative to the spacecraft). The intensity levels are captured in Table 1.

## CONTROLLER DESIGN

A top-level block diagram of the system dynamics is shown in Figure 5. The control system uses five output measurements: the relative positions of test mass 1 in X and Y; the relative positions of test mass 2 in X and Y; and the spacecraft attitude error from the star tracker. The five control inputs are the thruster force commands in X and Y, the thruster torque command, and the suspension control force commands on test mass 2 in X and Y. It is important to note that no suspension forces are applied to test mass 1. A 1% parasitic cross-talk between the X and Y axis suspension forces on test mass 2 is assumed in the analysis. There are two main control loops required for the spacecraft control. First is the drag-free controller, which controls the position of the spacecraft (in X and Y) to establish the drag-free motion of test mass 1. The second controller is the spacecraft attitude control, which is primarily designed to orient the spacecraft in the low frequency band (DC and near DC) using the star tracker data. However, it is also designed to center the spacecraft about test mass 2 in the transverse (Y) direction in the ST7 science measurement band from 1 to 10 mHz. Both test masses are effectively freely falling in the measurement band.

$$K_{al}(s) = \frac{b_2 s^2 + b_1 s + b_0}{s^5 + a_4 s^4 + a_3 s^3 + a_2 s^2 + a_1 s} \quad (5)$$

$$\begin{aligned} a_4 &= 6.568e-3 & b_2 &= 2.481e-12 \\ a_3 &= 2.157e-5 & b_1 &= 4.410e-16 \\ a_2 &= 4.148e-8 & b_0 &= 3.308e-20 \\ a_1 &= 3.990e-11 \end{aligned}$$

This controller provides a cut-off frequency of about 0.00005 Hz. The controller term  $K_{ah}(s)$  represents the part of the attitude controller that centers the spacecraft about test mass 2 in the transverse direction (Y-direction) in the ST7-DRS measurement band. This controller is also designed based on the classical approach, and is a series combination of lead-lag filter, PD filter, and a roll-off filter, resulting in a sixth-order controller with the following transfer function.

$$K_{ah}(s) = \frac{b_5 s^5 + b_4 s^4 + b_3 s^3 + b_2 s^2 + b_1 s + b_0}{s^6 + a_5 s^5 + a_4 s^4 + a_3 s^3 + a_2 s^2 + a_1 s + a_0} \quad (6)$$

$$\begin{aligned} a_5 &= 3.579 & b_5 &= 392.8 \\ a_4 &= 6.406 & b_4 &= 70.81 \\ a_3 &= 0.1596 & b_3 &= 0.1764 \\ a_2 &= 0.0015 & b_2 &= 1.658e-4 \\ a_1 &= 6.273e-06 & b_1 &= 6.934e-08 \\ a_0 &= 9.845e-09 & b_0 &= 1.088e-11 \end{aligned}$$

The relative X and Y position of test mass 2 is controlled by the electrostatic suspension control internal to the GRS. The relative position in X is controlled via a low bandwidth PID controller to provide disturbance rejection at DC and near DC. The Y-position control comprises two compensators. One is a low bandwidth PID controller to provide disturbance rejection at DC and near DC. The other is a feedforward compensator that nulls out the compensation effects of the low bandwidth attitude controller. This compensation removes a significant part of the coupling between the attitude loop and the 2<sup>nd</sup> test mass position control in Y, and therefore makes the system more amenable to decentralized control. It also naturally corrects for any disturbances caused in the test mass position control loop by attitude control commands. The structure of this controller is given by

$$u_{sy}(s) = K_{sy}(s)y_2(s) + h * K_{al}(s)\theta(s) \quad (7)$$

Here  $u_{sy}(s)$  denotes the suspension control force for test mass 2 in Y. The nominal controller,  $K_{sy}(s)$ , is a low-bandwidth PID loop, and the scaling constant  $h$  depends on the moment arm from spacecraft center of mass to the test mass, the spacecraft inertia, and the mass of the test mass.

## STABILITY MARGINS

Each of the controllers was designed to have sufficient stability margins. However the 7-DOF system represented in Figure 5 is a MIMO system, by virtue of the cross coupling between the relative test mass positions and the attitude of the spacecraft. Hence, the loop gains at each input and output channel (while the remaining channels are closed) must be analyzed to obtain proper stability margins. Figures 6–11 show the loop gains for six of the ten channels. The loop gains of the other four channels (the X and Y components of the relative positions of the two test masses) are virtually identical to four of the plots shown. Figure 9 shows that the Y-axis suspension force on test mass 2 is the loop exhibiting the minimum margins: 7.6 dB of gain margin and 35° of phase margin. These margins are amply sufficient considering that the effects of zero-order hold and computational and transport delays are already included in the analysis. The margins for the attitude pointing error shown in Figure 11 are similar to those for the Y-axis suspension force, which is driven by spacecraft attitude accelerations.

## ANALYSIS RESULTS

The attitude and drag-free controllers were implemented in a MATLAB-based model of the system that serves as the design and analysis tool for the 7-DOF Model. The results of both time-domain and frequency-domain analyses are shown in Figures 12–21. The root power spectral density plots show the contributions of the various disturbance sources. The contribution of each disturbance category represents the root sum squared (RSS) values for that category; for example, the thruster noise plot is the RSS contribution of the noise from all four thrusters.

Figures 12a–15a illustrate the root power spectral densities of the relative positions of both test masses, in both X and Y directions. These are dominated by the thruster noise and capacitive sensing measurement noise in the measurement bandwidth. The cross coupling that exists in this MIMO system may be observed in the variations in the contributions from different thruster noise sources, as well as the contribution of solar radiation pressure noise in the X direction. Both test masses satisfy the positioning requirement of  $10 \text{ nm}/\sqrt{\text{Hz}}$  in both directions in the science measurement band (the top of the plots for test mass 1 and indicated by horizontal lines for test mass 2), although the spacecraft only follows test mass 1. The necessity of controlling test mass 2 to follow the spacecraft over long time scales is reflected in the higher root power spectral densities of its relative position components at frequencies below the science measurement band. Figures 14a and 15a show that the star tracker measurement noise contributes significantly to the test mass 2 relative position errors below the science measurement band. Figures 12b–15b show 42-hour time histories of the relative positions of the two test masses, with the lower plot being an expansion of the last 1000 seconds. It can be seen that the displacement of test mass 1 never exceeds 4 nm, and only very occasionally exceeds 3 nm, in agreement with the frequency domain results. The displacement of test mass 2 shows larger low-frequency motions, also agreeing with the frequency domain results.

Figure 16 shows the root spectrum for the spacecraft pointing error, which indicates that the error is well within its requirement of  $1^\circ/\sqrt{\text{Hz}}$ . This error is also dominated by the thruster noise and capacitive measurement noise in the science measurement band and by star tracker measurement noise below the measurement band.

Figures 17–19 present the spectra and time histories of the thruster force commands in the X, Y and torque directions. The RSS levels are well within the  $20 \mu\text{N}$  capability of the colloidal thrusters. The major contributor to the spectra in and below the measurement band is thrust noise, while capacitive sensing noise becomes dominant well above the measurement band.

Figures 20 and 21 illustrate the spectra and time histories of the suspension control forces on test mass 2 in the X and Y directions, respectively; these are well within the  $10 \text{ nN}/\sqrt{\text{Hz}}$  capability of the electrostatic suspension system of the GRS. Thrust noise, capacitive sensing noise, and star tracker noise all have major contributions to the suspension force spectral densities, within and below the measurement bandwidth.

## DISCUSSION

The time-domain and frequency-domain analyses presented in this paper show that all the requirements for the ST7-DRS control system are met in a planar seven-degree-of-freedom model. These requirements include establishing drag-free motion of the test masses in the science band as well as spacecraft attitude control. The spacecraft position relative to the primary test mass will be maintained within the required precise limits. Successful spacecraft attitude control is accomplished by combining low frequency data from a star tracker and high frequency data from the transverse position of the second test mass. It was also proved that rapidly rolling off the electrostatic suspension forces on the second test mass between DC and the measurement frequency band provides adequate suspension while maintaining its drag-free state within the frequency range of interest. All these conclusions must be confirmed in a three-dimensional eighteen-degree-of-freedom dynamic model of the spacecraft and test masses. No essential complications are expected to arise at this level, however.

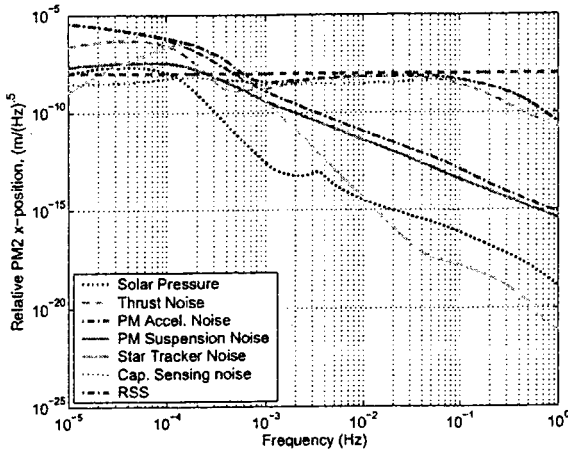


Figure 14a Root Power Spectrum of the Relative Position of Test Mass 2: X-Direction

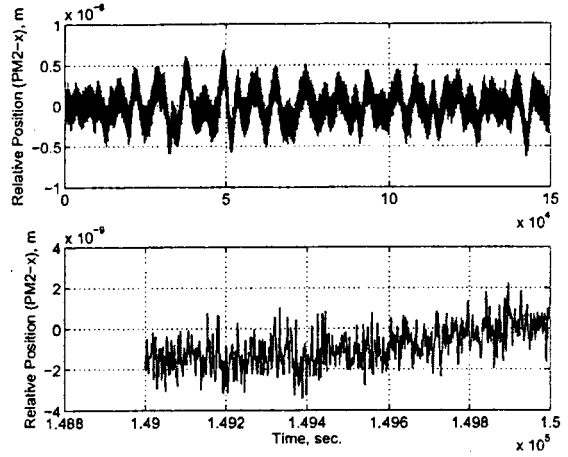


Figure 14b Time History for the Relative Position of Test Mass 2: X-Direction

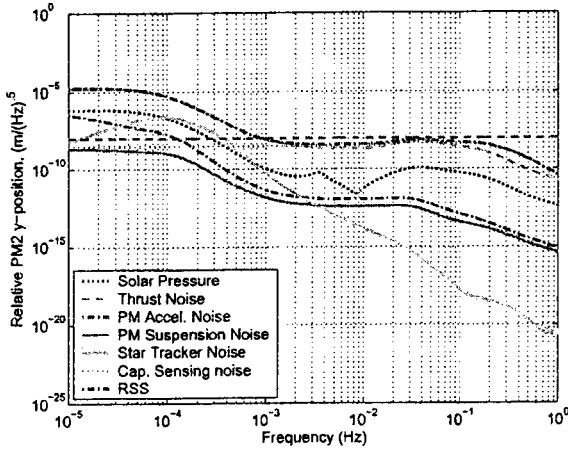


Figure 15a Root Power Spectrum of the Relative Position of Test Mass 2: Y-Direction

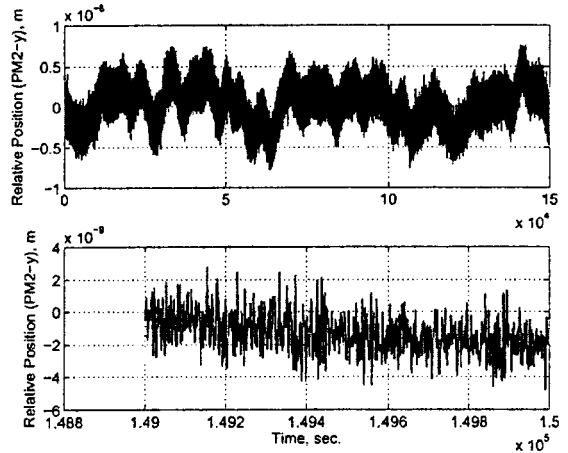


Figure 15b Time History for the Relative Position of Test Mass 2: Y-Direction

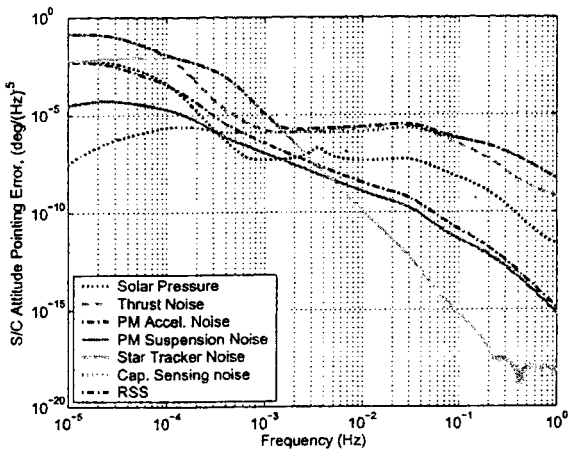


Figure 16a Root Power Spectrum of the Spacecraft Attitude Pointing Error

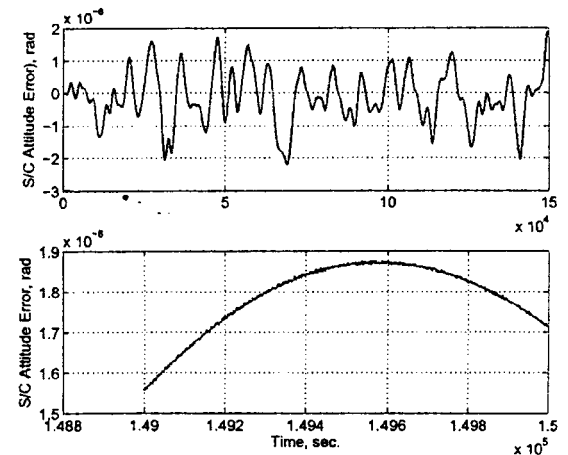


Figure 16b Time History for the Spacecraft Attitude Pointing Error

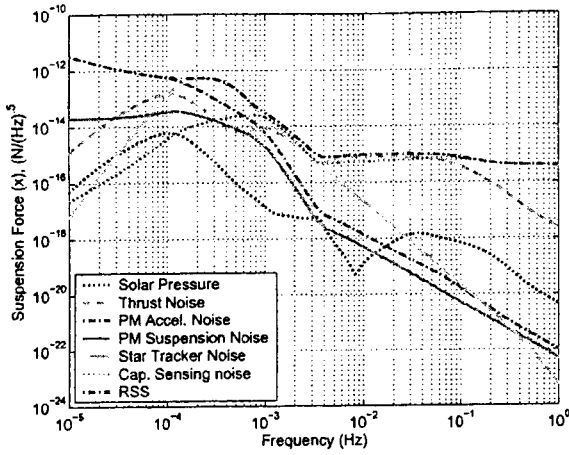


Figure 20a Root Power Spectrum of the X-axis Suspension Force on Test Mass 2

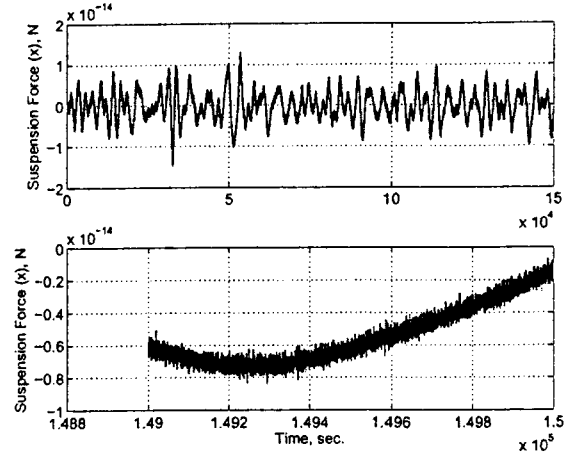


Figure 20b Time History for the X-axis Suspension Force on Test Mass 2

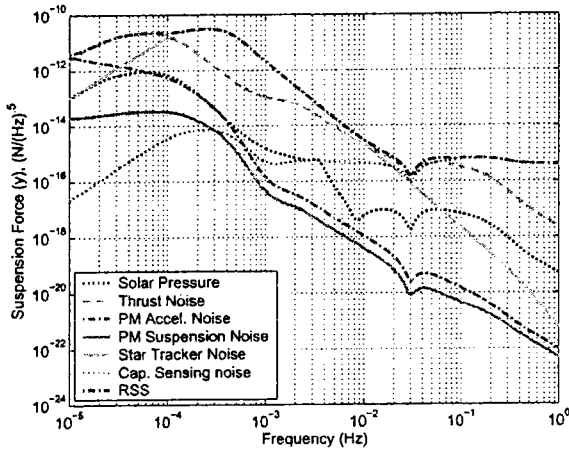


Figure 21a Root Power Spectrum of the Y-axis Suspension Force on Test Mass 2

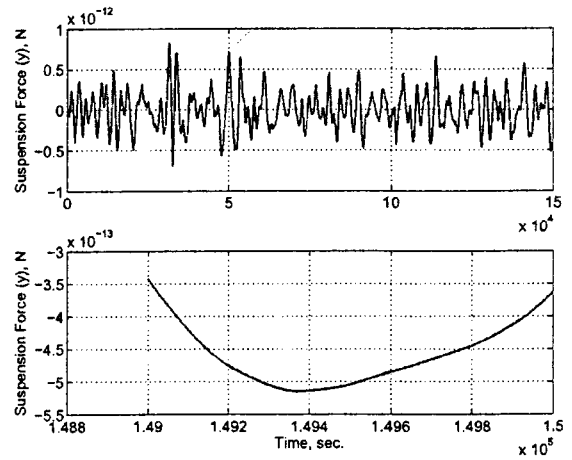


Figure 21b Time History for the Y-axis Suspension Force on Test Mass 2